PAPER PUBLISHED IN IEEE TRANSACTIONS ON AUTOMATION SCIENCE AND ENGINEERING, VOL. 19, NO. 2, APRIL 2022
https://dx.doi.org/10.1109/TASE.2021.3057433

A Synthetic Aperture UHF RFID Localization Method by Phase Unwrapping and Hyperbolic Intersection

Paolo Tripicchio , *Senior Member, IEEE*, Matteo Unetti , Salvatore D'Avella , *Student Member, IEEE*, Alice Buffi , *Member, IEEE*, Andrea Motroni , *Member, IEEE*, Fabio Bernardini , *Member, IEEE*, and Paolo Nepa , *Senior Member, IEEE*

***Abstract*— The use of radio frequency identification (RFID) technology for the traceability of products throughout the production chain, warehouse management, and the retail network is spreading in the last years, especially in those industries in line with the concept of Industry 4.0. The last decade has seen the development of increasingly precise and high-performance methods for the localization of goods. This work proposes a reliable 2-D localization methodology that is faster and provides a competitive accuracy, concerning the state-of-the-art techniques. The proposed method leverages a phase-distance model and exploits the synthetic aperture approach and unwrapping techniques for facing phase ambiguity and multipath phenomena. Trilateration applied on consecutive phase readings allows finding hyperbolae as the localization solution space. Analytic calculus is used to compute intersections among the conics that estimate the tag position. An algorithm computes intersections quality to select the best estimation. Experimental tests are conducted to assess the quality of the proposed strategy. A mobile robot equipped with a reader antenna localizes in 2-D the tags placed in an indoor scenario and reconstructs the map of the environment through a simultaneous localization and mapping (SLAM) algorithm.**

***Note to Practitioners*—A localization technology based on passive ultrahigh-frequency (UHF) radio frequency identification (RFID) is an enabling technology for intelligent warehouses, logistics, and retails. For this reason, this work presents a novel method to estimate the tag location with high accuracy. A reader antenna is mounted on an autonomous mobile robot that can move in an indoor or outdoor environment due to a simultaneous localization and mapping (SLAM) algorithm. The motion of the antenna generates a synthetic aperture. The system receives the phase measurements from the RFID tags and generates a distance model through phase unwrapping. In such a way, the possible locations of the tags in the environment are generated, creating conics. The trilateration step is performed analytically, intersecting the obtained conics. The resulting estimations are very accurate and not computation expensive. Therefore, the proposed approach can be employed in any application where localizing objects is fundamental even when reduced computational power is available, e.g., in warehouses where the products are at known heights, or where the items are placed on a fixed infrastructure, such as high-shelves logistics, to produce the inventory of the tagged objects within each shelf.**

***Index Terms*— Industry 4.0, mobile robot, phase unwrapping, radio frequency identification (RFID) localization, tag localization, warehouse logistics.**

I. Introduction

RADIO frequency identification (RFID) technology in the ultrahigh-frequency (UHF) spectrum is widely applied in industries in line with the concept of Industry 4.0, especially in the field of logistics and warehouse automation. In such scenarios, the passive RFID technology, due to its capacity of automated identification and data capture (AIDC), is suitable for tacking track of the incoming and outcoming products in the industry plants [1], for item-level tagging in retail stores [2], for localizing autonomous mobile robots that move goods in the plant [3], for autonomous robot manipulators that perform bin picking or packing tasks [4], for identifying materials properties [5], or as an intuitive and easy-to-operate method to navigate an unmanned aerial vehicle [6]. Furthermore, the passive UHF-RFID systems are well appreciated for their low cost and promising localization accuracy.

The working principle for locating a radio frequency (RF) signal generated by passive RFID tags consists of measuring either the received signal strength indicator (RSSI) or the phase of its backscattering signal. Several techniques were proposed in the literature for achieving adequate performance.

Digital Object Identifier 10.1109/TASE.2021.3057433

Hightower *et al.* [7] introduced a trilateration method exploiting a distance attenuation model on the RSSI. Since the accuracy of such a method was largely affected by multipath and reflections, Ni *et al.* [8] proposed the introduction of reference tags in the environment. The disadvantages of techniques exploiting reference tags are the need for a relatively high tag spatial-density and a full knowledge about the environment map. Recent approaches combine RSSI and signal phase [9], [10], but the current trend is to employ phase-only methods due to the favorable sensitivity of the phase to distance measurements.

Phase-based methods typically leverage the phase difference of arrival (PDOA) [11]. One of the main approaches is based on the angle of arrival (AOA) that can be extracted from the PDOA [12]. However, the distance between the receiving antennas should be lower than half wavelength to remove phase ambiguity, and high localization accuracy requires for large array antennas. Furthermore, strategies in which the antenna or the tag are moved according to a synthetic aperture radar (SAR) approach or its inverse form have been proposed [13], [14]. SAR methods provide good localization performance but usually require large computational costs. For this reason, they are suitable for off-line reconstruction algorithms [15]. Optimization techniques have been proposed especially for grid-based algorithms [16] to overcome this issue and to allow the online estimation of tags location even in large 3-D scenarios. Employing a virtual antenna array, Wang and Katabi [17] tried to solve the multipath issue by modeling the signal profiles of nearby RFIDs employing dynamic time warping (DTW) techniques. The antenna can be moved by a mobile robot in the environment allowing the sorting of RFID tags in libraries, manufacturing lines, or offices [18]. Instead, unwrapping algorithms, previously applied in interferometric SAR [19], image processing [20], and other fields, have been lately introduced in RFID localization [21] to eliminate the ambiguity of the phase cycle. Recently, Zhang *et al.* [22] proposed a Bayesian filter-based algorithm and a variable power RFID model for localizing passive UHF tags in complex environments. Li *et al.* [23] proposed a system to localize RFID tags on shelves by combining both RSSI and phase information acquired by two moving antennas with different orientations. The two RSSI values can be used to roughly determine the height of the tags on the shelf and to account for different possible orientations of the tag and surface materials to which the tag could be placed on. The phase data history is used to estimate the tag lateral location, by adopting a matching function, such as in SAR techniques, which also takes into account the quality of each phase samples in terms of the signal-to-noise ratio. In the work presented in [24], Bernardini *et al.* studied the exploitation of multiple synthetic apertures for improving static tag localization accuracy. In fact, in many real cases, the RFID tag could be interrogated in different time intervals associated with different inventories, thus having more than one available synthetic aperture to determine its location. Di Giampaolo and Martinelli [25] proposed an alternative model of SAR methods based on the concept of multiple baseline synthetic arrays. The proposed processing consecutively evaluates couples of phase samples by resembling two-element arrays with an increasing baseline. The goal of the method is to understand which phase samples are severely affected by multipath interference and exclude them from the final tag location estimation process. Real experiments showed the advantage of this method with respect to classical SAR processing in indoor environments. Zhao *et al.* [26] presented position error compensation (PEC), an accurate synthetic aperture RFID localization system with aperture PEC, which has a major advantage over the classical SAR techniques of not requiring the exact knowledge of the antenna trajectory. The method has been applied in an extensive experimental campaign, and results showed that it achieves the centimeter-level accuracy with aperture position error in noisy environments, proving its effectiveness and robustness. Jiang *et al.* [27] introduced a SAR-based multi-granularity system called RF-SML, to find the high-probability region of the target position by reconstructing the reflection coefficient and reducing the time-computational burden of the localization calculation. The authors conducted real experiments, and the results showed that the proposed method can efficiently achieve the centimeter-level positioning of items.

RFID localization has also been achieved employing hyperbolic positioning [28] to trilaterate the positions of tags and reader antenna. Recent studies address hyperbolic positioning as an optimization problem [29] to improve the cost-effectiveness of positioning systems.

The work here presented discusses a methodology for localizing passive UHF-RFID tags from a moving antenna carried on a robot. The method employs the mobile RFID reader antenna to form a synthetic array and uses a phase unwrapping algorithm to remove phase ambiguity. Hyperbolic positioning is adopted to compute tag-position candidates at every robot (antenna) location. Unlike previous works that employ multiple collinear antennas, a single antenna is used. The intersection between pairs of hyperbolae is obtained with an analytic method, and finally, an optimization criterion computes the best estimation of tag positions. The proposed approach achieves a centimeter-order localization error by using online computation.

This article is structured as follows. Section II introduces background concepts on phase measurements. In Section III, a detailed description of the methodology is presented explaining the unwrapping algorithm, the hyperbolae construction, their intersection computation, and the final location estimation. Section IV is dedicated to the experimental trial, results, and discussions. A conclusion section closes this contribution.

II. Signal Model

An RFID system consists of tags, a reader connected to one or more antennas, and a host management system. The reader antenna queries tags by sending an electromagnetic interrogation signal, and tags send back digital data that usually represent the electronic product code (EPC), univocally identifying the item that the tag is attached to. The host management system collects all the data received by the reader from several tags into the scenario. Passive tags are powered by energy from the reader interrogating radio waves; thus, the read range mainly depends on the chip sensitivity.

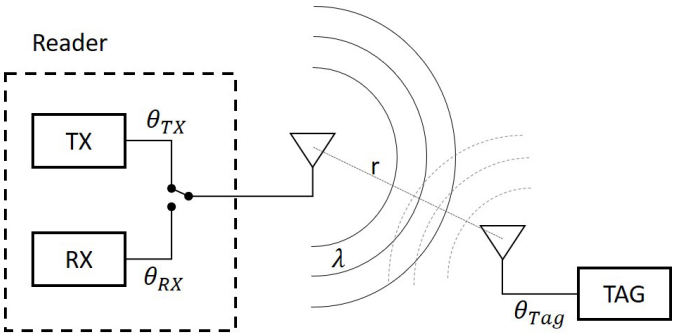

Fig. 1. Schematics of the RFID communication. r is the distance between the reader and tags antennas. θ_{TX}, θ_{RX}, and θ_{Tag} depend upon the electronic circuits and compose the phase offset ϕ_0.

More in detail, when an RFID reader antenna interrogates a passive tag, an RF signal providing command and power is transmitted to the tag, which, on activation, returns the modulated backscattering signal to the reader. The phase of the complex signal backscattered by the tag mainly depends on the distance between the tag and the reader antenna but also by the reader receiving and transmitting hardware circuits and the tag itself (see Fig. 1). The observed phase-distance model for the ith reading can be written as

$$\phi_i = \left(\phi_0 + \frac{2\pi}{\lambda}\, 2\, r\right) \bmod 2\pi \tag{1}$$

where λ is the free-space wavelength of the radiated field, ϕ_0 is the phase offset including the effect of cables and other reader components [30], and r is the distance traveled twice by the RF signal during the backscattering communication.

Equation (1) shows that the observed phase value ϕ_i is the remainder of the phase rotation to 2π, revealing that the observed value wraps and repeats over the $0 - 2\pi$ interval. Therefore, the same observed value could be obtained from multiple antenna distances, depending on the number of cycles, generating ambiguity. The process of extracting the distance information from that observed value must take this phenomenon into account. Furthermore, even the phase offset, ϕ_0, should be considered. Ma *et al.* [31] studied the effect of the phase offset ϕ_0 on SAR methods. The offset ϕ_0 is not perfectly constant but slightly varies since the antenna phase-center position changes according to the relative orientation between the antenna and tag [32]. By designing a proper calibration function for the ϕ_0 term, the accuracy of SAR localization methods can be increased. Another aspect that is worth mentioning is the modeling of the thermal noise that is usually treated as the Gaussian noise.

In Section III, the essay would discuss the methodology adopted to extract the distance information from the phase signal of the RFID, taking into account the issues of the distance-model in (1).

III. Methodology

A. Phase Unwrapping

Given an agent, being a mobile robot or a vehicle, equipped with a single reader antenna, and a tag positioned in the surrounding environment, when the agent moves, the relative distance r, between the tag and the antenna reader, varies along the path. A *phase history* can be acquired as the tag is interrogated multiple times by the moving reader antenna.

Considering the variations of the signal phase concerning the value assumed at a given reference time, namely, the *relative phase history* of the complex signal, the constant ϕ_0 (phase offset) can be removed from (1) since its variations are usually small in the tag proximity during the agent motion. The resulting equation is

$$\Delta\phi_i = \left(\frac{2\pi}{\lambda}\, 2\Delta r\right) \bmod 2\pi \tag{2}$$

where the Δ operator represents the difference between two phase samples (1) collected at two positions that are Δr apart.

Before applying the phase difference, it is required to remove the phase ambiguity to reconstruct the phase revolution. Thus, the unwrapping technique [33] has been applied to the measured phase (1). It adjusts the phase angles by adding multiple cycles when absolute jumps between consecutive phase samples are greater than or equal to the jump tolerance π. Naming the unwrapped phase ϕ^u, the procedure is equivalent to

$$\phi_0^u = \phi_0 \tag{3}$$

$$\phi_i^u = \phi_i - 2\pi * \left\lfloor \frac{\phi_i - \phi_{i-1}^u}{2\pi} + \frac{1}{2} \right\rfloor. \tag{4}$$

The constraint for the spatial sampling is chosen according to the Shannon theorem [34] that can be formulated as follows:

$$\Delta r \leq \frac{\lambda}{4\, \sin\left(\frac{1}{2}\, \omega_{\mathrm{hp}}\right)} \tag{5}$$

with ω_{hp} being the half-power beamwidth of the reader antenna. This relation guarantees that the difference between two adjacent phase samples is lower than π, which can prevent the phase unwrapping technique from failing. Successive readings are collected with nonuniform sampling following the EPC UHF Gen2 Air Interface Protocol Standard anticollision protocol [35]. However, if consecutive readings satisfy (5), the complex signal can be successfully reconstructed, and the tag position can be estimated without ambiguity. Fig. 2 shows an example of the unwrapped distance obtained from a phase history as

$$phiDist_i = \phi_i^u * \frac{\lambda}{4\pi}. \tag{6}$$

B. Hyperbolae Construction

Given a general scenario in which a tag is located at position RFid and the reader antenna is mounted on a robot moving from position AP_0 to position AP_1, as depicted in Fig. 3, the distance between the tag and AP_0 can be written as r and the distance between the tag and AP_1 as $r + \Delta r$. Knowing $\Delta\phi$, it is possible to obtain Δr via unwrapping. The distance d between AP_0 and AP_1 can be alternatively computed through the robot odometry or a more precise simultaneous localization and mapping (SLAM) algorithm [36]. Nevertheless, the only unknown variable to solve the localization problem is the distance r that will be found by circles intersection.

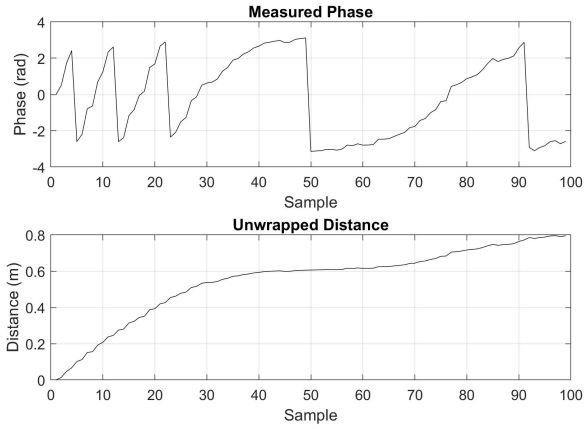

Fig. 2. Unwrapped distance values obtained from the corresponding measured phase history.

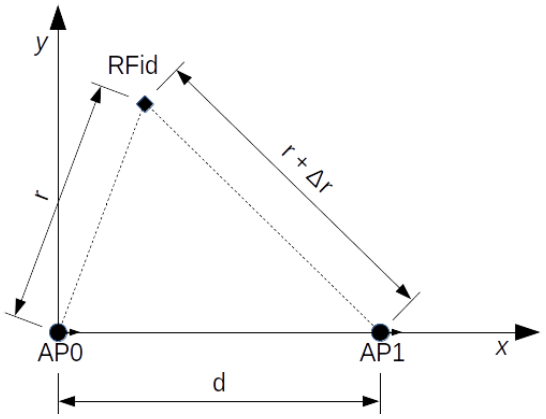

Fig. 3. Scenario depicting the antenna motion from the position AP_0 to the position AP_1. An RFID tag is located at position $RFid$.

Choosing a value R as guess for r, it is possible to generate a circle with radius R centered in AP_0 and a circle with radius $R + \Delta r$ centered in AP_1. In the most general case, the circles will intersect in two points that are symmetric with respect to the $\overline{AP_0AP_1}$ segment. A unique solution would exist if $2R + \Delta r = d$, while no solution can be found if $2R + \Delta r < d$.

The locus of all possible intersections can be obtained varying the value of R iteratively. The solution of this procedure is a hyperbola by definition, and its mathematical model is derived by analytic calculus. The reference frame is at the center of the $\overline{AP_0AP_1}$ segment, and the y-axis would be orthogonal to it, as shown in Fig. 4.

The circles equations in the chosen reference frame are

$$\left(x + \frac{d}{2}\right)^2 + y^2 = R^2 \tag{7}$$

$$\left(x - \frac{d}{2}\right)^2 + y^2 = (R + \Delta r)^2. \tag{8}$$

Moving to polar coordinates, x and y become

$$x = R\cos\alpha - \frac{d}{2} \tag{9}$$

$$y = R\sin\alpha \tag{10}$$

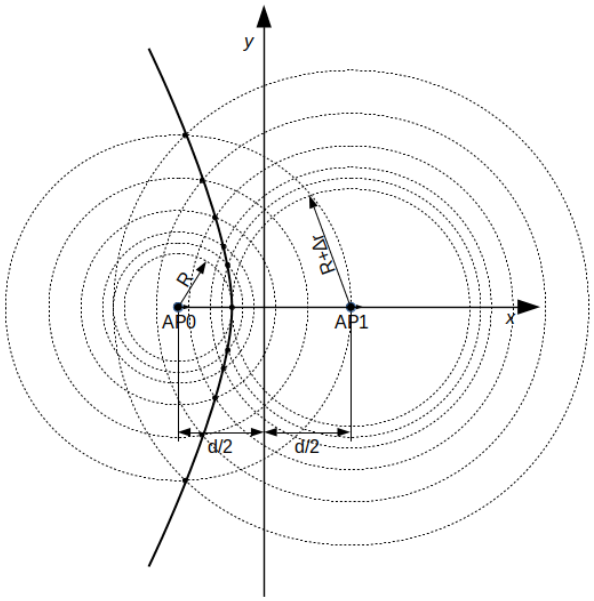

Fig. 4. Procedure to obtain the locus of all possible circles intersection and an exemplary hyperbola obtained from it.

and substituting them in (8), it is possible to write

$$R = \frac{d^2 - \Delta r^2}{2(\Delta r + d\cos\alpha)}. \tag{11}$$

The hyperbola equation in the canonical form is formulated as

$$\frac{x^2}{a^2} - \frac{y^2}{b^2} = 1. \tag{12}$$

Choosing a point with coordinate $y = 0$ ($\cos\alpha = 1$), the a parameter is obtained

$$a = \pm\frac{\Delta r}{2}. \tag{13}$$

Finally, using the equation of the asymptotes, which is

$$\frac{y}{x} = \frac{b}{a} \tag{14}$$

and posing the denominator of (11) equal to 0, it is possible to find the parameter b

$$b = \pm\frac{\sqrt{d^2 - \Delta r^2}}{2}. \tag{15}$$

C. Reference-Frame Transformations

Computing the distance d as the norm of the $\overline{AP_0AP_1}$ segment and Δr from the phase unwrapping procedure, it is possible to obtain the locus of the possible tag locations that have generated such phase measurement, as depicted in Fig. 4. Then, it is necessary to transform such a locus on a global reference frame for performing the computation of the intersection between a pair of hyperbolae. Such a transformation is described in the following steps.

The first step involves the formulation of the hyperbola in matrix form. Given a vector $X = [x, y, 1]$, it is possible to

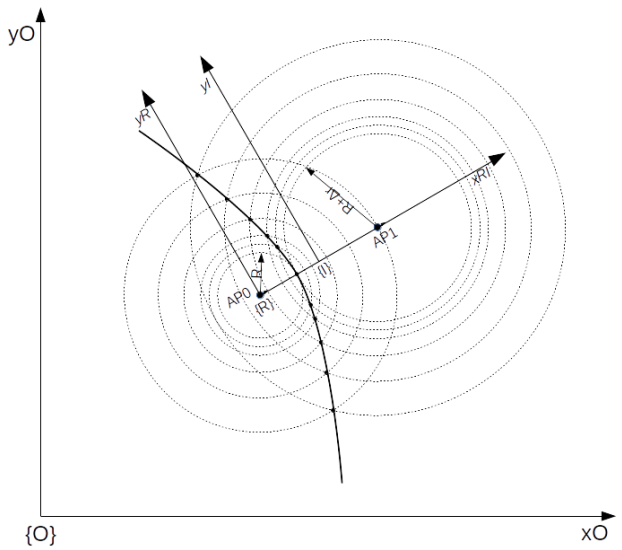

Fig. 5. Hyperbola represented in the global reference frame $\{O\}$.

write a generic conic as $X\,A\,X^T$. In that case, the matrix A will assume the values

$$A = \begin{bmatrix} \frac{1}{a^2} & 0 & 0 \\ 0 & -\frac{1}{b^2} & 0 \\ 0 & 0 & -1 \end{bmatrix}. \tag{16}$$

Referring to Fig. 5, the matrix A represents the hyperbola in the reference frame $\{I\}$. The following translation is applied to move from the reference frame $\{I\}$ to the reference frame $\{R\}$:

$$T_1 = \begin{bmatrix} 1 & 0 & -\frac{d}{2} \\ 0 & 1 & 0 \\ 0 & 0 & 1 \end{bmatrix}. \tag{17}$$

Then, a rotation is applied to align the xR axis with the xO axis. The rotation angle θ can be obtained as $\text{atan2}(AP_{1y} - AP_{0y}, AP_{1x} - AP_{0x})$, resulting in the rotation matrix

$$R_1 = \begin{bmatrix} \cos\theta & \sin\theta & 0 \\ -\sin\theta & \cos\theta & 0 \\ 0 & 0 & 1 \end{bmatrix}. \tag{18}$$

Finally, another translation T_2 is applied to center the conic in the reference $\{O\}$

$$T_2 = \begin{bmatrix} 1 & 0 & -AP_{0x} \\ 0 & 1 & -AP_{0y} \\ 0 & 0 & 1 \end{bmatrix}. \tag{19}$$

The conic expressed in the matrix form in the global reference frame $\{O\}$ is obtained multiplying the matrix transformations, as follows:

$$C_0 = T_2^T\, R_1^T\, T_1^T\, A\, T_1\, R_1\, T_2. \tag{20}$$

D. Conics Intersection

Given two hyperbolas with matrices C_0 and C_1, to numerically compute their intersections, it is possible to build a pencil that contains both the conics

$$C_\lambda = C_0 + \lambda C_1. \tag{21}$$

It is worth noticing that the intersection points $p = (x, y)$ lie on C_λ for any value of λ

$$p^T\, C_\lambda\, p = 0 \quad \forall\, \lambda. \tag{22}$$

Furthermore, there exists a special conic of the pencil that is represented by straight lines intersecting both the intersection points. Such lines are a degenerate conic whose matrix determinant is null ($\det(C_\lambda) = 0$).

Equation (21) can be reformulated as follows:

$$C_\lambda (C_1)^{-1} = \lambda I - C_0(-C_1)^{-1} = \lambda I - B. \tag{23}$$

In this formulation, λ represents the eigenvalues of B. Solving the characteristic polynomial $\det(\lambda I - B) = 0$, λ can be found, and it is possible to compute the degenerate conic C_d by substitution. C_d can be further decomposed as the multiplication of two lines, as follows:

$$C_d = l_1^T\, l_2 + l_2^T\, l_1. \tag{24}$$

Intersecting the obtained lines with one of the two conics of (21), (C_0 or C_1), it is possible to find the intersection points

$$p_1^T\, C_0 = l_1 \tag{25}$$

$$p_2^T\, C_0 = l_2. \tag{26}$$

E. Localization Algorithm

Starting from an initial position of the reader antenna AP_0 and a nominal distance $phiDist_0$ derived from the unwrapped phase history, a new conic is generated according to the above formulations for any movement of the robot, and hence the antenna, greater than an assigned stride size. Concurrently, a vector containing the current position of the reader antenna and the current unwrapped phase distance is stored. The next step of the algorithm performs the intersection between the novel hyperbola and all the previously obtained hyperbolae.

Fig. 6 shows an example of multiple hyperbolae obtained moving the antenna in seven different positions and their intersection. The ground-truth position of the tag (red circle) does not belong to any computed hyperbola due to the phase measurement noise. During each step of the antenna motion, a vector containing the (x, y) coordinates of the intersection (*posRFID*), the unwrapped phase distance $phiDist_n$, and an estimation of the quality of the localization guess (E) would be allocated for each resulting intersection point.

The quality estimation is computed as

$$E = \sum_{i=0}^{N} \sum_{k=i+1}^{N} Q_{k,i} \tag{27}$$

$$Q_{k,i} = \|\Delta_{k,i}(D) - \Delta_{k,i}(phiDist)\| \tag{28}$$

$$\Delta_{k,i}(D) = D_i - D_k \tag{29}$$

$$\Delta_{k,i}(phiDist) = phiDist_i - phiDist_k \tag{30}$$

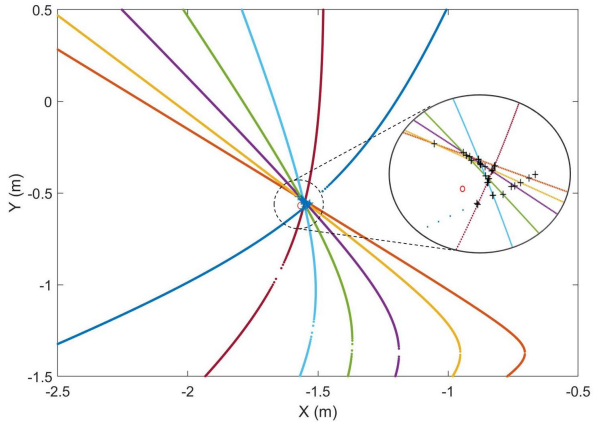

Fig. 6. Intersection between different conics to obtain the best estimation of an RFID tag location. The red circle is the ground-truth tag position and the black X the analytic hyperbolae intersections.

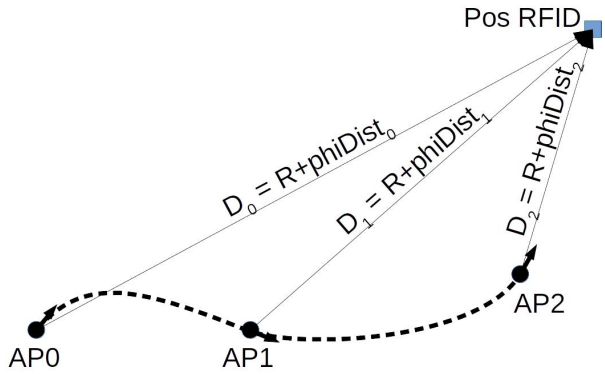

Fig. 7. Measurements involved in the estimation of the quality of the localization guess *PosRFID*.

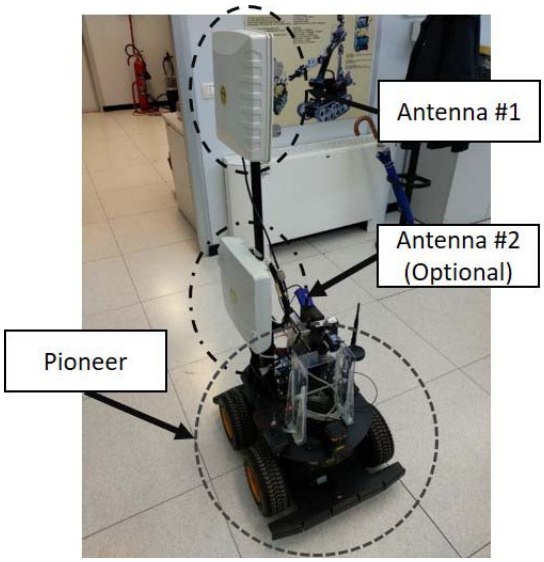

Fig. 8. Experimental setup showing the mobile robot and the mounted antennas.

where D_i is the distance between *PosRFID* and the ith position of the antenna AP_i along the trajectory, and D_k is the same parameter by considering the kth position of the antenna, with $k \neq i$. In particular, *PosRFID* denotes any generic intersection found between a pair of hyperbolas, whereas $D_0, D_1, \ldots, D_N$ are the distances between *PosRFID* and all the previous reader antenna locations (known due to SLAM or other methods), and $phiDist_i$ are the distances derived by unwrapping the phase samples (6). Fig. 7 gives a graphical view of all the measures involved in the computation.

Considering, for instance, the positions AP_2 and AP_1 of the reader antenna, it is possible to write the following equation:

$$D_2 - D_1 = R + phiDist_2 - R - phiDist_1 \quad (31)$$

$$= phiDist_2 - phiDist_1. \quad (32)$$

This means that, if the estimation is exact, $Q_{1,2} = 0$.

Therefore, the solution of the localization problem is the best estimation of the tag position, obtained finding the point $posRFID^*$ that minimizes the objective function E

$$posRFID^* = \arg\min_{(x,y)\in\Theta} \left(\sum_{i=0}^{N} \sum_{k=i+1}^{N} Q_{k,i} \right) \quad (33)$$

where Θ is the set of all the found hyperbola intersections. We initially considered performing the computation of an average of the intersections to obtain the best estimation guess, but this resulted in increased computational time and in no real advantage on accuracy. This is due to the fact that the average will not probably belong to any of the conics, and thus, it will present a systematic error.

IV. Experiments and Discussion

An extensive measurement campaign was carried out in an indoor scenario employing a Pioneer 3-AT UGV manufactured by MobileRobots equipped with specialized UHF-RFID hardware. In particular, an Impinj Speedway Revolution R420 [37] reader was installed on the UGV along with two circularly polarized WANTENNAX019 antennas by C.A.E.N. RFID [38]. The first and second antennas have been placed at 125 and 75 cm in height, respectively. Fig. 8 shows the mobile robot equipped with the two reader antennas. Only the first antenna is used in the following tests.

The robot is skid-steering with a four-wheel drive and can rotate on the place with zero radius. It has an array of 16 sonars arranged along the four sides and a computer connected to a microcontroller. The robot uses the microcontroller to interface with the motors and manage the odometer update and the obstacle detection, by using the sonar sensors. Laser data have been captured employing a Hokuyo laser range finder (LRF) (UTM-30LX).

Thirty-eight passive UHF-RFID tags have been placed in an office environment within a volume of 7 m $\times$ 5 m $\times$ 1.5 m with different orientations, as depicted in Fig. 9. Several tag typologies using the Impinj Monza R6 chip (with a sensitivity of -22.1 dBm) were employed. An external multicamera tracking system, i.e., Vicon MX [39], has been used to obtain ground-truth measurements. The Vicon system utilizes a set of calibrated cameras working in the infrared spectrum to acquire, by triangulation, the space position of markers whose surface is covered by an infrared retroreflective tape with a maximum acquisition rate of 240 Hz. Through the use of eight

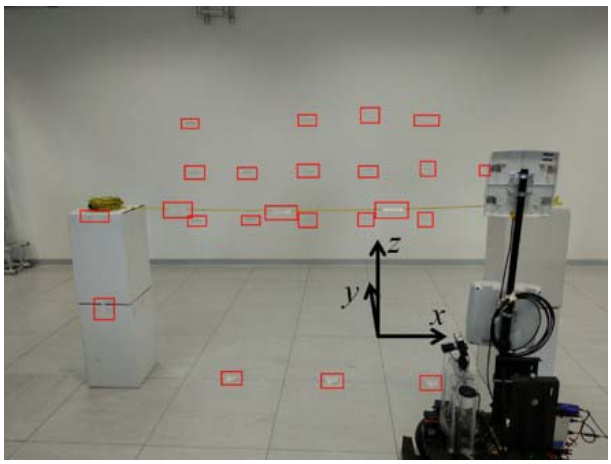

Fig. 9. Experimental setup where the tests have been conducted. The positions of the RFID tags that are visible in the picture are highlighted by red boxes.

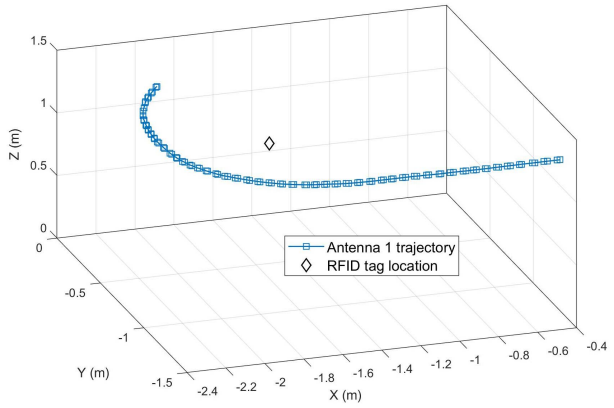

Fig. 10. Trajectory performed by antenna 1 during the robot motion inside the indoor environment and exact position of an RFID tag placed in $P_{\text{tag}} = [-1.564; -0.569; 1.013]$ m as reported by the Vicon system.

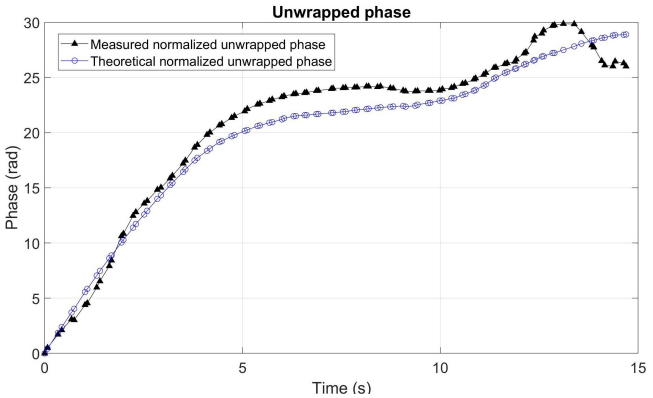

Fig. 11. Measured unwrapped phase curve (black triangular markers) and theoretical unwrapped phase curve (blue circular markers), gathered when the antenna moves according to the trajectory of Fig. 10 while detecting the RFID tag in $P_{\text{tag}} = [-1.564, -0.569, 1.013]$ m. All phase measurements are normalized with respect to the first reading sample.

calibrated cameras, it was possible to track the antenna motion and determine the position of the tags with an error of less than 1 mm. Optical markers have been placed at tag positions to obtain their absolute location before the experimental phase. Furthermore, a marker was also attached to each antenna for tracking the motion of the antennas during the experiments inside the Vicon workspace.

The reader input power was set to $P_{\text{TX}} = 27$ dBm, and the measurements were acquired at a frequency of $f_0 = 865.7$ MHz (ETSI Channel 4).

A. Single-Tag Scenario

In the following, a single tag positioned at $P_{\text{tag}} = [-1.564, -0.569, 1.013]$ m is considered. The reader antenna number 1, employed in this test, moves from point $AP_1 = [-0.428, -1.370, 1.253]$ m to point $AP_{99} = [-1.960, -0.165, 1.253]$ m acquiring 99 readings. Fig. 10 shows the antenna 1 trajectory as reconstructed by the Vicon system and the tag location. The corresponding synthetic aperture is $L = [1.79, 1.3]$ m. The corresponding measured unwrapped phase curve (black triangular markers) is presented in Fig. 11. The theoretical unwrapped phase curve (blue circular markers) computed as in (1) by exploiting the ground-truth trajectory measured by the Vicon system has also been added. All phase measurements are normalized with respect to the first reading sample to overcome the phase offset issue. The phase unwrapping was done through a MATLAB function, which is suitable when the reader antenna travels at low velocity and condition (5) is met. The difference between the two curves is mainly due to the multipath effects. Indeed, the oscillations present in the last part of the measured curve clearly indicate the presence of multipath components affecting the RFID measurements and excited by metallic structure where the Vicon cameras were mounted, nearby walls, ceiling, and floor.

By choosing a minimum stride of 30 cm for the conics generation, only ten hyperbolae are generated, resulting in a total of 42 computed intersections. Fig. 12 depicts a boxplot with scatter points of the estimation error for each intersection point in the XY plane concerning the RFID tag position guess. Among statistical data, the sample values are shown, and the worst and best estimation guesses are highlighted. The best estimation has been correctly selected by the proposed criteria in (33).

It is worth noticing that all the computed intersections give an estimation of the tag position within a 5-cm distance error. The localization error is always computed in the 2-D plane as the magnitude of the difference between the projection of the real tag position (ground truth) in the xy plane (reader antenna plane) and the best estimation of the algorithm (in the xy plane) following the simple formula:

$$error = \|tag\_position - posRFID^*\|. \tag{34}$$

The ideal case is to have both the reader antenna and the tag at the same height coordinate to reduce the effects of the error due to the projection of the actual distance onto the antenna plane (Fig. 13). However, the proposed method shows good robustness capabilities concerning the projection error that is due to the different heights between the reader antenna and the

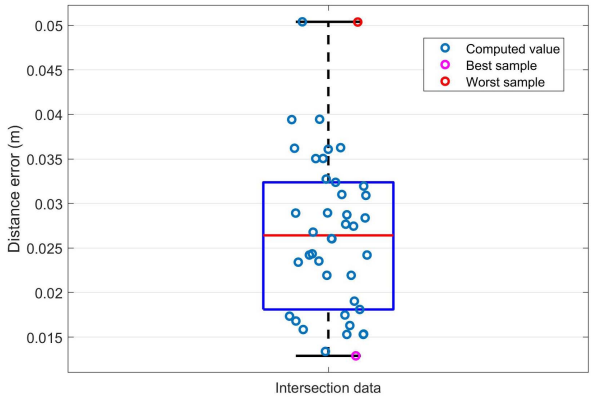

Fig. 12. Boxplot and scatter values of distance errors between the ground-truth tag position and the estimation computed at each intersection of the generated hyperbolae. The scatter points are randomly distributed on the abscissa to improve visibility. The best sample correctly selected by the proposed algorithm is highlighted in pink.

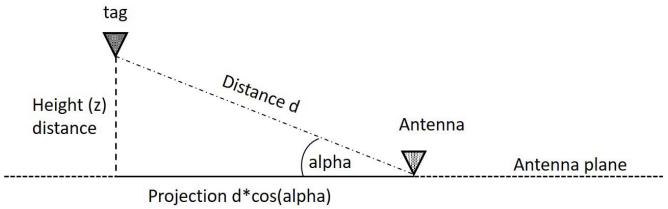

Fig. 13. Projection of the distance on the antenna plane seen from the side view (z-axis up).

tags. By analytically computing the error of the measurement of the tag position from the antenna position P_1, considering 25 cm of height difference and a distance of nearly 1.5 m, the resulting projection on the antenna plane would present a 2-cm error. Repeating such an analysis for the closest point of the trajectory, given the smaller distance of the reader antenna from the tag, an error of 7 cm would be obtained. Nonetheless, the proposed localization algorithm is able to improve the tag position estimation (reaching an error of nearly 1.3 cm) since it basically exploits the information coming from several phase samples.

While the method is suitable for a single antenna usage, employing multiple antennas may allow obtaining greater precision on the 2-D projection if the tags are located at different heights in a warehouse or a shop (typically on shelves). The second antenna, mounted on the robot 50 cm lower than the first antenna, generates similar error metrics resulting in a tag position guess of 1.6 cm.

B. Influence of the Antenna Height

To assess the influence that the antenna height has on the algorithm accuracy, a test has been run in simulation. In this case, no multipath effects are considered, and the generated phase signals are combined with a zero-mean Gaussian noise with 0.1-rad standard deviation. The simulation involves a tag at a fixed x- and y-coordinates (3 m, 0 m) and varying its z-coordinate between 0 and 1.5 m, at 0.25-m intervals. The receiving antenna is supposed to move on a plane with a z-coordinate equal to 0. This experiment is aimed to show how

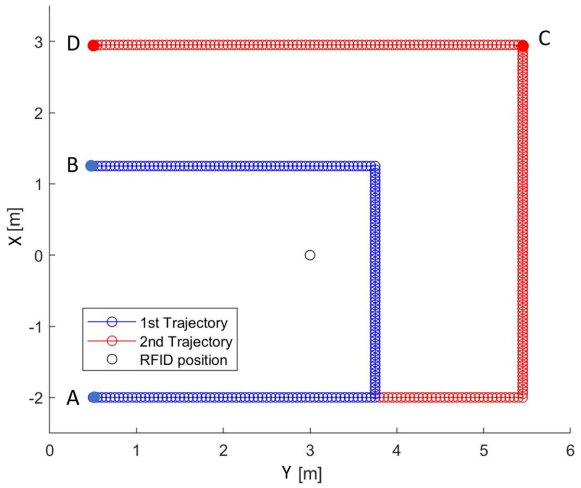

Fig. 14. RFID position and paths of the RFID antenna in the simulations test as seen on the xy plane. Three trajectories are defined: from point A to point B, from point A to point C, and from point A to point D.

the projection error affects the localization accuracy depending on the height difference between the tag and the antenna. Two other conditions are taken into account: these are the length of the antenna trajectory, and the distance of the trajectory from the tag. In the simulation, the antenna moves along two different paths (see Fig. 14): the first path is composed of 200 steps of 0.05 m, each covering a total length of 10 m (from A to B), while the second path is composed of 300 steps of 0.05 m, each covering a total length of 15 m (from A to D). The third trajectory is considered moving the antenna on the second path but stopping after 200 steps at point C. The resulting error for each height difference on the three trajectories is reported in Table I. The table reports the mean and the standard deviation of the localization accuracy obtained from a set of 100 Monte Carlo simulations for each combination of the above conditions. From the results, it is possible to analyze the change in the localization error due to the different heights of the antennas and the influence of the distance of the trajectory from the tag and the influence of the trajectory length on the estimation error. Results show that with the increase in the height difference between the antenna and the tag, the tag 2-D estimation error increases. This result was expected due to the influence of the projection from 3-D coordinates to 2-D coordinates and the relative error. The obtained results are in line with the results obtained from the single-tag experiment (where the antennas had nearly 0.25-m height difference with respect to the tag).

C. Influence of the Antenna Trajectory Distance and Length

Looking again at the results shown in Table I, it is possible to state that, if the motion of the antenna occurs with an increased distance from the tag, the error induced by the projection is mitigated. The same consideration holds if the trajectory of the antenna is elongated. In this sense, the final accuracy of the localization appears more sensible to the length, geometry, and distance of the observation path than to the antenna-height difference. This suggests that the antenna

TABLE I

RFID POSITION ESTIMATION ERROR (AND STD) AT VARYING HEIGHTS WHEN THE ANTENNA MOVES ON THREE DIFFERENT TRAJECTORIES

Tag height	Error $\mu\,(\sigma)$ on Trajectory (A-B)	Error $\mu\,(\sigma)$ on Trajectory (A-C)	Error $\mu\,(\sigma)$ on Trajectory (A-D)
0 m	0.42 (0.20) cm	0.42 (0.23) cm	0.38 (0.19) cm
0.25 m	1.14 (0.42) cm	0.58 (0.22) cm	0.39 (0.22) cm
0.5 m	4.26 (0.47) cm	1.25 (0.26) cm	0.79 (0.37) cm
0.75 m	8.98 (0.93) cm	2.66 (0.56) cm	1.62 (0.30) cm
1.0 m	13.84 (0.95) cm	4.01 (1.88) cm	2.70 (0.36) cm
1.25 m	20.59 (1.11) cm	7.42 (0.54) cm	4.55 (0.32) cm
1.5 m	23.71 (1.53) cm	9.26 (2.48) cm	5.60 (0.16) cm

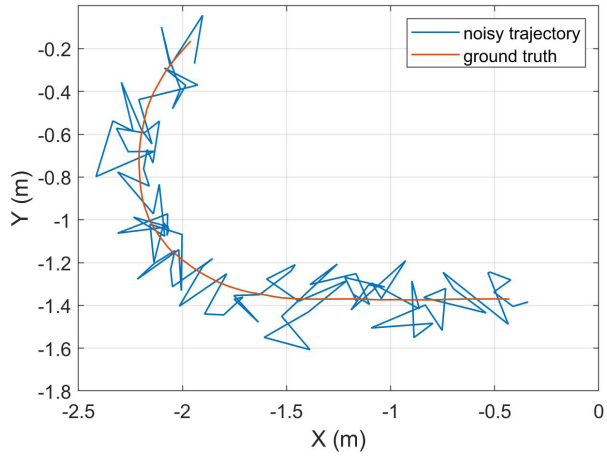

Fig. 15. Ground-truth trajectory of the single-tag scenario (red) compared to a generated trajectory with added Gaussian noise $\mathcal{N}(0, 0.1)$ (blue).

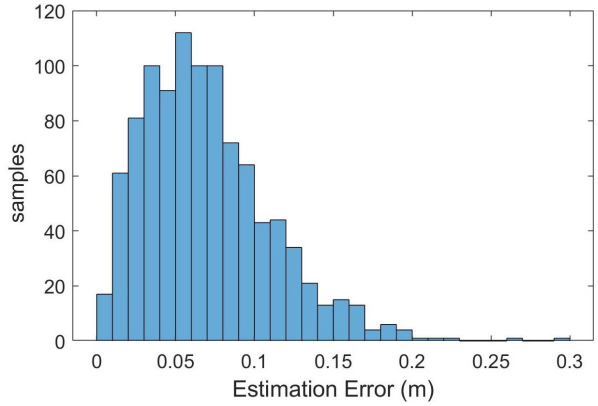

Fig. 16. Histogram of the estimation error on 1000 Monte Carlo simulations.

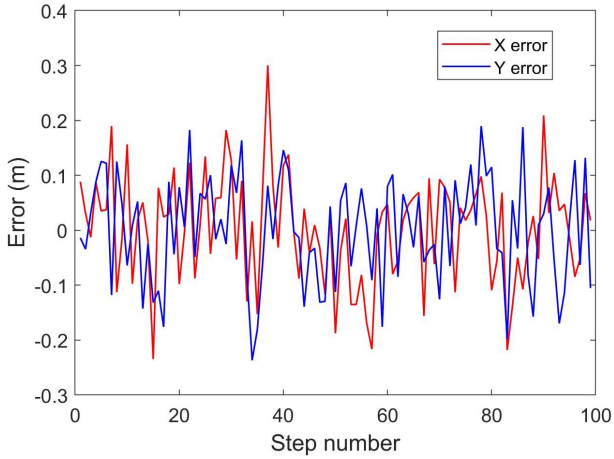

Fig. 17. Errors between the ground-truth trajectory and the generated trajectory shown in Fig. 15.

trajectory should be planned carefully to obtain a bounded error and a desired accuracy on the localization.

D. Influence of the Robot Position Accuracy

In the single-tag scenario, the ground-truth trajectory captured from the Vicon system has been used for robot motion knowledge. In this paragraph, a study on how reconstruction errors in the antenna (robot) motion could affect the accuracy of the tag localization is presented. This discussion is beneficial to understand if simple motion estimation algorithms, such as dead reckoning or cheap sensing solutions usually embedded in handheld devices, could be used as antenna localization modules. In particular, the algorithm has been run based on a trajectory produced by altering the ground-truth trajectory by adding the Gaussian noise with a standard deviation of 0.1 m. To reach statistical significance, the algorithm has been executed on 1000 different simulations. Fig. 15 shows one exemplary trajectory compared to the ground-truth one, while Fig. 16 shows a histogram of the resulting errors. The median error is 6.4 cm, but the major concentration is around 5 cm. This shows that even with a large estimation error of the antenna motion (see Fig. 17), the resulting accuracy is bounded.

E. Multiple-Tag Scenario

A more exhaustive testing session was performed to assess the accuracy of the presented method when varying orientation, spatial distribution, typology, and distance of the tags. In these tests, the entire set of 38 tags has been employed. Tags orientations vary from 0° to 90° in all the spatial directions (x, y, and z). They have been attached to a planar wall, on a line on the ground, over the faces of two carton semicolumns, and on a tight rope (see Fig. 9). The three tags on the floor have been used as a reference to align the Vicon system with the robot and RFID measures and are not considered in the following location computation statistics. The antenna mounted on the robot moved in the environment performing almost circular trajectories around the semicolumns and the rope, in 11 different testing sessions. The distance of the tags from the reader antenna varied accordingly in the range 0.12 m $\leq R \leq$ 5.74 m. Fig. 18 shows the distribution of the tags in a 3-D graphic along with one of the reconstructed trajectories of the reader antenna.

The robot motion and the relative trajectories of the antenna have been computed through an SLAM algorithm that fuses the odometry readings from the wheel-mounted encoders and the inertial measurement unit (IMU) with a scan matching procedure performed on laser data [40].

The problem solved by the SLAM algorithm is to simultaneously determine a good estimation of the vehicle pose and represent the operating environment where the vehicle lays with a map. The map is usually represented as a set of landmarks or features. The choice of proper features depends

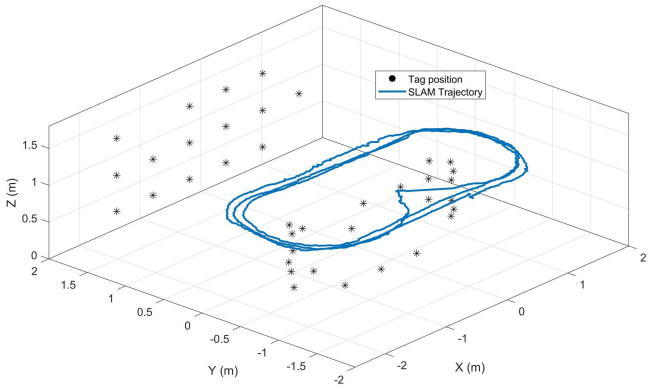

Fig. 18. Trajectory performed by the antenna on a testing session during the robot motion and tags placement on the environment.

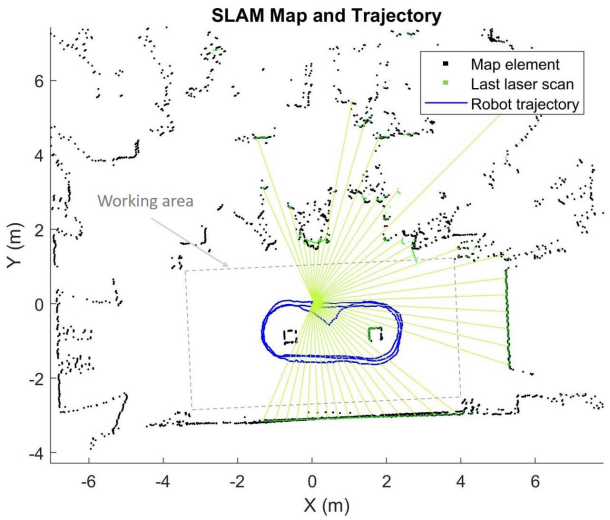

Fig. 19. Environment map and robot trajectory of a testing session obtained from an SLAM procedure combining odometry, inertial, and laser measurements.

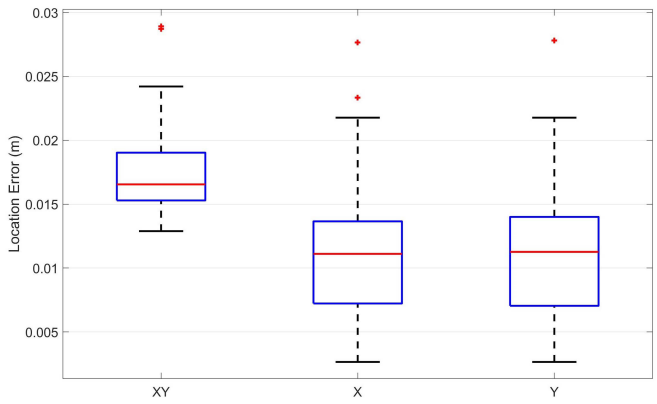

Fig. 20. Variation of the position estimation error considering different tags orientations, positions, and types.

on the available sensors. In the case of LRF sensors, it is practical to select points or lines as features for describing the environment [41].

Fig. 19 presents the result of the SLAM procedure showing the reconstructed environment map obtained from the laser readings and the estimated robot trajectory. The implemented SLAM method can reconstruct the trajectory within a centimeter error, which is comparable to the accuracy obtained from other techniques for localizing mobile robots that have been proven reliable in indoor exploration and inspection scenarios where the GPS signal is not available [42], [43]. According to the analysis carried out in Section IV-D and considering that the accuracy of the employed SLAM method is of centimeter order, the robot position estimation should not worsen the RFID location estimation.

The test environment is a portion of a larger open space laboratory room. As can be inferred from the reconstructed map, the office has some openings, and contextually, some people were moving in the portion not involved in the test during the acquisition. Nevertheless, the SLAM procedure is robust enough to obtain good accuracy performance even in the presence of noisy inputs due to people's motion and light artifacts caused by daylight entering from office windows.

For what concerns the RF signals, the environment poses severe multipath conditions due to the presence of walls, columns, metallic structures, and desks with personal computers located inside the laboratory room.

Statistics of the tag location estimation errors for the eleven reconstructed trajectories of the robot antenna are reported in Fig. 20. The figure shows the boxplot of the error in the x-coordinate (X), the error in the y-coordinate (Y), and the Cartesian error ($XY = (X^2 + Y^2)^{1/2}$). The slight difference between the error in the x- and y-coordinates concerns the distribution of the tags and the performed trajectories. Nevertheless, the Cartesian error remains bounded with small variations around the mean value.

A comparison of accuracy and computation time of the proposed method with the state-of-the-art techniques that use similar approaches is reported in Table II. In particular, the timing performance measurement has been conducted on an Intel Core i3 M380 at 2.53 GHz to be consistent with the timings obtained by Wu *et al.* [21]. The rows with a light gray background report results as they were computed in the referenced works and are here reported to show the most relevant results using synthetic aperture, hyperbolic positioning, and unwrapping. The last two rows present results obtained in the discussed environment that is much larger than in the other papers. In particular, the SARFID [15] method has been applied using a uniform grid partitioning of 3 cm in the bounding volume between the coordinates $(-2.5, -1.5, -0.1)$ and (2, 2, 1.6) m.

Results confirm that the computational time is greatly reduced in contrast to grid-based methods with the same dimensionality when employing the unwrapped phase-distance model. The computational time is further reduced with respect to iterative optimization methods by employing an analytical approach for finding the intersection of the conics. Consideration should be done on the timing of the algorithm. Although the computational burden of matrix multiplications is relatively small and optimized in the machine, the number of hyperbolas and, thus, intersections could potentially explode in the case of long trajectories. However, when the motion trajectory starts

TABLE II
COMPARISON OF DIFFERENT METHODS AT THE STATE OF THE ART CONCERNING BOTH THE 2-D LOCATION ERROR AND THE TIMING PERFORMANCE (TOP). RESULTS OF METHODS APPLIED ON THE MULTIPLE-TAG SCENARIO (BOTTOM)

Previous results from Literature	Localization error μ_{xy} (σ_{xy})	Computational time μ (σ)
SAR in [13]	10.05 cm (9.42 cm)	1120.2 ms (21.0 ms)
Hyperbolic in [29]	13.23 cm (2.23 cm)	N.A.
Unwrapped in [21]	**9.96 cm (9.6 cm)**	**14.7 ms (10.7 ms)**
Methods applied on tested Scenario	**Location error μ_{xy} (σ_{xy})**	**Computation time μ (σ)**
SARFID [15]	10.44 cm (140.58 cm)	13.9 ms (17.0 ms)
Proposed method	**1.76 cm (0.4 cm)**	**7.8 ms (5.3 ms)**

increasing, it is possible to reduce the computational time considering, during the intersection computation, a limited number of hyperbolae instead of all the generated conics, thus lowering the timing demands. The selection can be done based on geometrical considerations (e.g., approaches similar to GDOP [44] of GPS) or unwrapping techniques. The more the unwrapping is unrolled, the more the phase error is reduced. In addition, taking into consideration the lobe apertures, many points can be directly deleted. Finally, taking advantage of the quality estimation algorithm, it is efficiently convenient to maintain an array of the most promising hyperbolae and perform the computations only on them, so further lowering the computational time.

Concerning the accuracy of the method, the difference with previous results could be explained by the fact that the proposed method considers all the possible $N(N-1)/2$ hyperbolae being N the acquired phase readings, which cannot be done in [28], since the number of hyperbolae is related to the number of antennas, while, with the method in [29] with N readings, only $N-1$ hyperbolae are considered. Increasing such a lot the number of hyperbolae leads to a method more robust to noise and multipath phenomena. Concerning [21], the introduction of an analytical solution leads to a method more robust to noise and multipath.

Analyzing the results of the proposed scenario, the better estimation with respect to the SARFID method is probably the result of severe multipath effects in the measurements that more affect the SARFID estimation since this method is not properly a maximum-likelihood estimator and does not perform well in low signal-to-noise ratio scenarios [45].

F. Limitations of the Method and Usage Guidelines

Major drawbacks for the effective usage of the proposed method are due to phase measurements related problems. In fact, many noise sources may combine during RFID tag readings due to multipath or interference. During the experiments, in some cases, the unwrapping step has been difficult due to the low sample spatial density. Indeed, if no holes are present and the unwrapping lasts for many samples, the errors due to noise are mitigated. When holes break the unwrapping in small parts that relates to small robot motions, the measurement error (0.1 rad + positioning error) could lead to a large estimation error that may invalidate the computed intersections. When the robot moves slowly, usually, the phase measurements are quite continuous. However, a few guidelines could be followed to ensure the robustness of the proposed system to noise measurements. First, it has been shown that larger motion paths allow for a better estimation of the tags' locations (see Section IV-B). In fact, longer trajectories motion means wider acquisitions (synthetic antenna apertures) and smaller plane projection error. A second hint is that repeating the robot's motion several times (in our experiments, the robot performed some loops around the environment) allows the system to reacquire some measurements and to discard wrong readings in favor of better quality ones. In this context, RSSI values can be used to select only those samples with RSSI values greater than an assigned threshold.

G. Extension to 3-D Localization

Although most warehouse logistic applications just require 2-D localization techniques, given the knowledge of the environments where the goods are stored, some approaches to 3-D localization can be found in the recent literature. Motroni *et al.* [46] employ synthetic apertures and a robot platform to estimate the 3-D location of RFID tags by processing the tag backscattered signal phase data collected from two RFID reader antennas without requiring reference tags or large phased array antennas. A reduced computational cost with respect to classical SAR-based methods has been achieved in real-time 3-D positioning with the application of the particle swarm optimization in multiple-antenna SAR-based localization methods [47]. Tzitzis *et al.* [48], after introducing a post-processing phase called Phase ReLock [49], propose a novel method for 3-D RFID tags localization deploying a single RFID antenna on a robotic platform and forcing the robot to follow nonstraight paths, to elegantly solve the localization problem. Tests are performed on a planar surface and the estimation error in the z-coordinate results larger than for other coordinates. In a successive work [50], the same authors obtain a mean 3-D error of 35 cm in a scenario involving tags placed on different vertical planes. Liang *et al.* [51] developed E3DinSAR as an optimized Interferometric SAR-based 3-D localization approach for pinpointing tags rapidly and easily with a mean locating accuracy of 18.4 cm in 3-D space. E3DinSAR uses only one movable reader with one antenna.

Starting from the original approach here presented for 2-D tag localization, an extension of the method to 3-D localization that makes use of a dual antenna setup will be investigated in future work. A possible approach could be to match the planar intersections obtained separately from each antenna and estimate a 3-D location.

V. CONCLUSION

This work proposed a reliable 2-D localization method that shows robustness to the tested conditions and competitive performances concerning existing solutions in the literature.

The proposed method combines different techniques: the PDA based on the phase-distance model; SAR approach; phase-unwrapping for eliminating the phase ambiguity; definition of hyperbolas as localization solution space; closed-form

analytical expressions for computing intersection among the conics; and SLAM to localize the antenna mounted on the robot and to construct the map of the environment. By exploiting the useful properties of each of such techniques, the presented method achieves a mean accuracy of centimeter order and is suitable for online computation since its computation time is under the millisecond. Those results are the outcomes of an experimental campaign conducted in a $7\ \text{m} \times 5\ \text{m} \times 1.5\ \text{m}$ laboratory space employing different kinds of tags, located in different positions and orientations, a reader antenna mounted on a mobile robot, and a Vicon system used to construct the ground truth of the experiments.

REFERENCES

[1] R. Angeles, "RFID technologies: Supply-chain applications and implementation issues," *Inf. Syst. Manage.*, vol. 22, no. 1, pp. 51–65, Dec. 2005.

[2] G. M. Gaukler, R. W. Seifert, and W. H. Hausman, "Item-level RFID in the retail supply chain," *Prod. Oper. Manage.*, vol. 16, no. 1, pp. 65–76, Jan. 2007.

[3] P. R. Wurman, R. D'Andrea, and M. Mountz, "Coordinating hundreds of cooperative, autonomous vehicles in warehouses," *AI Mag.*, vol. 29, no. 1, p. 9, 2008.

[4] S. D'Avella, P. Tripicchio, and C. A. Avizzano, "A study on picking objects in cluttered environments: Exploiting depth features for a custom low-cost universal jamming gripper," *Robot. Comput.-Integr. Manuf.*, vol. 63, Jun. 2020, Art. no. 101888. [Online]. Available: http://www.sciencedirect.com/science/article/pii/S0736584519307276

[5] B. Xie *et al.*, "Tagtag: Material sensing with commodity RFID," in *Proc. 17th Conf. Embedded Netw. Sensor Syst. (SenSys)*, New York, NY, USA, Nov. 2019, pp. 338–350, doi: 10.1145/3356250.3360027.

[6] J. Zhang *et al.*, "RFHUI: An RFID based human-unmanned aerial vehicle interaction system in an indoor environment," *Digit. Commun. Netw.*, vol. 6, no. 1, pp. 14–22, Feb. 2020. [Online]. Available: http://www.sciencedirect.com/science/article/pii/S2352864818302694

[7] J. Hightower, R. Want, and G. Borriello, "Spoton: An indoor 3D location sensing technology based on RF signal strength," Dept. Comput. Sci., Univ. Washington, Seattle, WA, USA, Tech. Rep. 2000-02-02, Feb. 2000.

[8] L. M. Ni, Y. Liu, Y. C. Lau, and A. P. Patil, "LANDMARC: Indoor location sensing using active RFID," in *Proc. 1st IEEE Int. Conf. Pervasive Comput. Commun. (PerCom)*, Mar. 2003, pp. 407–415.

[9] H. Ma and K. Wang, "Fusion of RSS and phase shift using the Kalman filter for RFID tracking," *IEEE Sensors J.*, vol. 17, no. 11, pp. 3551–3558, Jun. 2017.

[10] Y. Zhao, K. Liu, Y. Ma, Z. Gao, Y. Zang, and J. Teng, "Similarity analysis-based indoor localization algorithm with backscatter information of passive UHF RFID tags," *IEEE Sensors J.*, vol. 17, no. 1, pp. 185–193, Jan. 2017.

[11] P. V. Nikitin, R. Martinez, S. Ramamurthy, H. Leland, G. Spiess, and K. V. S. Rao, "Phase based spatial identification of UHF RFID tags," in *Proc. IEEE Int. Conf. RFID (IEEE RFID)*, Apr. 2010, pp. 102–109.

[12] S. Azzouzi, M. Cremer, U. Dettmar, R. Kronberger, and T. Knie, "New measurement results for the localization of UHF RFID transponders using an angle of arrival (AoA) approach," in *Proc. IEEE Int. Conf. RFID*, Apr. 2011, pp. 91–97.

[13] R. Miesen, F. Kirsch, and M. Vossiek, "UHF RFID localization based on synthetic apertures," *IEEE Trans. Autom. Sci. Eng.*, vol. 10, no. 3, pp. 807–815, Jul. 2013.

[14] L. Yang, Y. Chen, X.-Y. Li, C. Xiao, M. Li, and Y. Liu, "Tagoram: Real-time tracking of mobile RFID tags to high precision using cots devices," in *Proc. 20th Annu. Int. Conf. Mobile Comput. Netw. (MobiCom)*, New York, NY, USA, 2014, pp. 237–248, doi: 10.1145/2639108.2639111.

[15] A. Motroni, P. Nepa, P. Tripicchio, and M. Unetti, "A multi-antenna SAR-based method for UHF RFID tag localization via UGV," in *Proc. IEEE Int. Conf. RFID Technol. Appl. (RFID-TA)*, Sep. 2018, pp. 1–6.

[16] F. Bernardini, A. Motroni, P. Nepa, A. Buffi, P. Tripicchio, and M. Unetti, "Particle swarm optimization in multi-antenna SAR-based localization for UHF-RFID tags," in *Proc. IEEE Int. Conf. RFID Technol. Appl. (RFID-TA)*, Sep. 2019, pp. 291–296.

[17] J. Wang and D. Katabi, "Dude, where's my card?: RFID positioning that works with multipath and non-line of sight," in *Proc. ACM SIGCOMM Conf. (SIGCOMM)*, New York, NY, USA, Aug. 2013, pp. 51–62, doi: 10.1145/2486001.2486029.

[18] L. Shangguan and K. Jamieson, "The design and implementation of a mobile RFID tag sorting robot," in *Proc. 14th Annu. Int. Conf. Mobile Syst., Appl., Services (MobiSys)*, New York, NY, USA, Jun. 2016, pp. 31–42, doi: 10.1145/2906388.2906417.

[19] M. A. Schofield and Y. Zhu, "Fast phase unwrapping algorithm for interferometric applications," *Opt. Lett.*, vol. 28, no. 14, pp. 1194–1196, 2003.

[20] S. M.-H. Song, S. Napel, N. J. Pelc, and G. H. Glover, "Phase unwrapping of MR phase images using Poisson equation," *IEEE Trans. Image Process.*, vol. 4, no. 5, pp. 667–676, May 1995.

[21] H. Wu, B. Tao, Z. Gong, Z. Yin, and H. Ding, "A fast UHF RFID localization method using unwrapped phase-position model," *IEEE Trans. Autom. Sci. Eng.*, vol. 16, no. 4, pp. 1698–1707, Oct. 2019.

[22] J. Zhang, Y. Lyu, J. Patton, S. C. G. Periaswamy, and T. Roppel, "BFVP: A probabilistic UHF RFID tag localization algorithm using Bayesian filter and a variable power RFID model," *IEEE Trans. Ind. Electron.*, vol. 65, no. 10, pp. 8250–8259, Oct. 2018.

[23] C. Li *et al.*, "ReLoc: Hybrid RSSI- and phase-based relative UHF-RFID tag localization with COTS devices," *IEEE Trans. Instrum. Meas.*, vol. 69, no. 10, pp. 8613–8627, Oct. 2020.

[24] F. Bernardini *et al.*, "Robot-based indoor positioning of UHF-RFID tags: The SAR method with multiple trajectories," *IEEE Trans. Instrum. Meas.*, vol. 70, pp. 1–15, 2021.

[25] E. DiGiampaolo and F. Martinelli, "A multiple baseline approach to face multipath," *IEEE J. Radio Freq. Identificat.*, vol. 4, no. 4, pp. 314–321, Dec. 2020.

[26] R. Zhao, D. Wang, Q. Zhang, H. Chen, and H. Xu, "PEC: Synthetic aperture RFID localization with aperture position error compensation," in *Proc. 16th Annu. IEEE Int. Conf. Sens., Commun., Netw. (SECON)*, Jun. 2019, pp. 1–9.

[27] Y. Jiang, Y. Ma, H. Liu, and Y. Zhang, "RF-SML: A SAR-based multi-granular and real-time localization method for RFID tags," *Electronics*, vol. 9, no. 9, p. 1447, Sep. 2020.

[28] T. Liu, L. Yang, Q. Lin, Y. Guo, and Y. Liu, "Anchor-free backscatter positioning for RFID tags with high accuracy," in *Proc. IEEE Conf. Comput. Commun. (INFOCOM)*, Apr. 2014, pp. 379–387.

[29] H. Ma, Y. Wang, K. Wang, and Z. Ma, "The optimization for hyperbolic positioning of UHF passive RFID tags," *IEEE Trans. Autom. Sci. Eng.*, vol. 14, no. 4, pp. 1590–1600, Oct. 2017.

[30] K. Finkenzeller, *RFID Handbook: Radio-Frequency Identification Fundamentals and Applications*. Hoboken, NJ, USA: Wiley, 1999.

[31] Y. Ma, H. Liu, Y. Zhang, and Y. Jiang, "The influence of the nonideal phase offset on SAR-based localization in passive UHF RFID," *IEEE Trans. Antennas Propag.*, vol. 68, no. 8, pp. 6346–6354, Aug. 2020.

[32] A. Buffi *et al.*, "UHF-RFID localization: The problem of antenna phase center in phase-based methods," in *Proc. 13th Eur. Conf. Antennas Propag. (EuCAP)*, 2019, pp. 1–5.

[33] Mathworks. *Unwrap*. Accessed: Nov. 5, 2020. [Online]. Available: https://www.mathworks.com/help/matlab/ref/unwrap.html

[34] C. E. Shannon, "Communication in the presence of noise," *Proc. IRE*, vol. 37, no. 1, pp. 10–21, Jan. 1949.

[35] *EPC UHF Gen2 Air Interface Protocol Standard*. Accessed: Nov. 5, 2020. [Online]. Available: https://www.gs1.org/epcrfid/epc-rfid-uhf-air-interface-protocol/2-0-1

[36] P. Tripicchio, M. Unetti, N. Giordani, C. A. Avizzano, and M. Satler, "A lightweight SLAM algorithm for indoor autonomous navigation," in *Proc. Australas. Conf. Robot. Automat. (ACRA)*, 2014, pp. 2–4.

[37] M. Lenehan, "Low level user data support," Speedway Revolution Reader, Impinj, Seattle, WA, USA, Appl. Note 2013-09-11 Revision 3.0, 2013.

[38] CAEN RFID. (2018). *Wantennax019—ETSI*. [Online]. Available: https: // www.caenrfid.com/en/products/wantennax019/

[39] (2019). *V System*. [Online]. Available: https://www.vicon.com/

[40] P. Biber and W. Strasser, "The normal distributions transform: A new approach to laser scan matching," in *Proc. IEEE/RSJ Int. Conf. Intell. Robots Syst. (IROS)*, vol. 3, Oct. 2003, pp. 2743–2748.

[41] G. Pepe, M. Satler, and P. Tripicchio, "Autonomous exploration of indoor environments with a micro-aerial vehicle," in *Proc. Workshop Res., Educ. Develop. Unmanned Aerial Syst. (RED-UAS)*, Nov. 2015, pp. 43–52.

[42] M. Satler, M. Unetti, N. Giordani, C. A. Avizzano, and P. Tripicchio, "Towards an autonomous flying robot for inspections in open and constrained spaces," in *Proc. IEEE 11th Int. Multi-Conf. Syst., Signals Devices (SSD14)*, Feb. 2014, pp. 1–6.

[43] P. Tripicchio, M. Satler, M. Unetti, and C. A. Avizzano, "Con-fined spaces industrial inspection with micro aerial vehicles and laser range finder localization," *Int. J. Micro Air Vehicles*, vol. 10, no. 2, pp. 207–224, Jun. 2018.

[44] I. Sharp, K. Yu, and Y. J. Guo, "GDOP analysis for positioning system design," *IEEE Trans. Veh. Technol.*, vol. 58, no. 7, pp. 3371–3382, Sep. 2009.
[45] N. Decarli, "On phase-based localization with narrowband backscatter signals," *EURASIP J. Adv. Signal Process.*, vol. 2018, no. 1, pp. 1–12, Dec. 2018.
[46] A. Motroni, F. Bernardini, P. Nepa, P. Tripicchio, and M. Unetti, "Towards a multi-antenna approach for UHF-RFID tag 3D localization with a synthetic aperture radar method," in *Proc. 4th Int. Conf. Smart Sustain. Technol. (SpliTech)*, Jun. 2019, pp. 1–7.
[47] F. Bernardini *et al.*, "Particle swarm optimization in SAR-based method enabling real-time 3D positioning of UHF-RFID tags," *IEEE J. Radio Freq. Identificat.*, vol. 4, no. 4, pp. 300–313, Dec. 2020.
[48] A. Tzitzis, S. Megalou, S. Siachalou, E. Tsardoulias, T. Yioultsis, and A. G. Dimitriou, "3D localization of RFID tags with a single antenna by a moving robot and 'Phase ReLock,"' in *Proc. IEEE Int. Conf. RFID Technol. Appl. (RFID-TA)*, Sep. 2019, pp. 273–278.
[49] A. Tzitzis *et al.*, "Localization of RFID tags by a moving robot, via phase unwrapping and non-linear optimization," *IEEE J. Radio Freq. Identificat.*, vol. 3, no. 4, pp. 216–226, Dec. 2019.
[50] A. Tzitzis *et al.*, "Trajectory planning of a moving robot empowers 3D localization of RFID tags with a single antenna," *IEEE J. Radio Freq. Identificat.*, vol. 4, no. 4, pp. 283–299, Dec. 2020.
[51] X. Liang, Z. Huang, S. Yang, and L. Qiu, "E3DinSAR: 3-D localization of RFID-tagged objects based on interference synthetic apertures," *IEEE Internet Things J.*, vol. 7, no. 12, pp. 11656–11666, Dec. 2020.

Paolo Tripicchio (Senior Member, IEEE) received the master's degree in automation engineering from the University of Pisa, Pisa, Italy, in 2006, and the Ph.D. degree *(cum laude)* in perceptual robotics from the Sant'Anna School of Superior Studies, Pisa, Italy, in 2012.

He is an Assistant Professor at the Department of Excellence in Robotics and AI, TeCIP Institute, Scuola Superiore Sant'Anna, Pisa. He was an Invited Lecturer at the Orizaba Institute of Technology, Orizaba, Mexico, in 2012, teaching classes on virtual reality and its applications. In 2016, he taught computer vision for autonomous drones at the Autonomous University of Toluca (UNAM), Toluca, Mexico. Since January 2013, he has been the Scientific Program Manager at the Gustavo Stefanini Advanced Robotics Research Center, La Spezia, Italy, dedicated to the advancements in mobile and field robotics. His main research areas cover different technological topics, such as studies on robotic perception, applications and theories of computer vision, AI systems and their applications, human–machine interaction with a particular focus on haptics, the fast-growing industrial robotics sector, field robotics applications, and the use of virtual and augmented reality for visualization, interaction, and simulation.

Matteo Unetti received the M.Sc. degree in automation engineering from the University of Pisa, Pisa, Italy, in 2003.

He is currently a Research Fellow with Gustavo Stefanini Advanced Robotics Research Center, a joint research center between Scuola Superiore Sant'Anna (SSSA) and Leonardo Company (formerly Finmeccanica) on mobile robots. His research activity concerns robotics, sensor fusion, localization, computer vision, and control systems.

Salvatore D'Avella (Student Member, IEEE) received the bachelor's degree in computer engineering from the University of Pisa, Pisa, Italy, and the master's degree in embedded computer systems from the Sant'Anna School of Advanced Studies, Pisa, where he is currently pursuing the Ph.D. degree in perceptual robotics with the Department of Excellence in Robotics and AI.

His main research areas are computer vision, artificial intelligence, and robotic, applied to Industry 4.0, especially for quality inspection and logistics.

Alice Buffi (Member IEEE) received the B.S. and M.S. *(summa cum laude)* degrees in telecommunications engineering and the Ph.D. (Doctor Europaeus) degree in applied electromagnetism in electrical and biomedical engineering, electronics, smart sensors, and nanotechnologies from the University of Pisa, Pisa, Italy, in 2006, 2008, and 2012, respectively.

In 2011, she was a Visiting Ph.D. Student with the Queen Mary University of London, London, U.K. Since 2012, she has been with the University of Pisa, where she is currently an Associate Professor with the Department of Energy, Systems, Territory and Construction Engineering. She has coauthored several international journal papers and international conference contributions, one European patent, and one European patent application. Her research topic includes measurement methods to locate static or moving items through radio frequency identification (RFID) systems operating at the ultrahigh-frequency (UHF) band in Industry 4.0 scenarios. Besides, she has interests in classification methods for smart gates and smart storage systems and the aging process in battery cells.

Dr. Buffi is a member of the IEEE Instrumentation and Measurement Society and the Antennas and Propagation Society. She was a recipient of the Best Paper Award at the IEEE RFID-TA 2019 International Conference and the Young Scientist Award from the International Union of Radio Science, Commission B, in 2013 and 2016, respectively. She serves as an Associate Editor for the IEEE JOURNAL OF RADIO FREQUENCY IDENTIFICATION.

Andrea Motroni (Member, IEEE) received the B.E. and M.E. *(summa cum laude)* degrees in telecommunications engineering from the University of Pisa, Pisa, Italy, in 2015 and 2017, respectively, where he is currently pursuing the Ph.D. degree in information engineering.

His research interests include indoor radio localization systems (with a specific focus on UHF RFID phase-based algorithms), passive RFID sensing, and RFID applications for the Internet of Things and Industry 4.0. He has coauthored one Italian patent application.

Fabio Bernardini (Member, IEEE) received the B.E. and M.E. degrees in telecommunications engineering from the University of Pisa, Pisa, Italy, in 2016 and 2018, respectively, where he is currently pursuing the Ph.D. degree in information engineering.

His research interests include indoor radio localization systems (with a specific focus on UHF-RFID phase-based algorithms), passive RFID sensing, and RFID applications for the Internet of Things and Industry 4.0.

Dr. Bernardini has been the President of the IEEE Student Branch of Pisa since February 2020.

Paolo Nepa (Senior Member, IEEE) received the Laurea degree *(summa cum laude)* in electronics engineering from the University of Pisa, Pisa, Italy, in 1990.

Since 1990, he has been with the Department of Information Engineering, University of Pisa, where he is currently a Full Professor. In 1998, he was a Visiting Scholar at the Electro Science Laboratory (ESL), The Ohio State University (OSU), Columbus, OH, USA, where he was involved in efficient hybrid techniques for the analysis of large antenna arrays. In the context of UHF-RFID systems, he is working on techniques for radio localization of either tagged objects or readers. He is also affiliated with the Italian National Research Council (CNR), Institute of Electronics, Computer and Telecommunication Engineering (IEIIT). He has coauthored more than 300 international journal articles and conference contributions. His research interests include the design of wideband and multiband antennas, and antennas optimized for near-field coupling and focusing.

Dr. Nepa is a member of the Technical Advisory Board of URSI Commission B—Fields and Waves. He was a recipient of the Young Scientist Award from the International Union of Radio Science, Commission B, in 1998. He served as the General Chair for the IEEE RFID-TA 2019 International Conference. Since 2016, he has been serving as an Associate Editor for the IEEE ANTENNAS AND WIRELESS PROPAGATION LETTERS.